Journal of the European Ceramic Society xxx (2017) xxx–xxx

Contents lists available at www.sciencedirect.com

Journal of the European Ceramic Society

journal homepage: www.elsevier.com/locate/jeurceramsoc

Full Length Article

Low-temperature co-sintering for fabrication of zirconia/ceria bi-layer electrolyte via tape casting using a Fe_2O_3 sintering aid

A.S. Mehranjani[a,*], D.J. Cumming[a], D.C. Sinclair[b], R.H. Rothman[a,*]

[a] Department of Chemical and Biological Engineering, University of Sheffield, Sheffield, S1 3JD, United Kingdom
[b] Department of Materials Science and Engineering, University of Sheffield, Sheffield, S1 3JD, United Kingdom

ARTICLE INFO

Article history:
Received 25 February 2017
Received in revised form 10 May 2017
Accepted 11 May 2017
Available online xxx

Keywords:
Co-sintering
YSZ/GDC bilayer
Interface
Interdiffusion
Solid oxide electrolysis cell

ABSTRACT

Bilayer electrolytes have potential in solid oxide cells to improve ionic conduction whilst blocking electronic conduction. GDC/YSZ bilayer electrolyte processing has proven problematic due to thermochemical instability at high sintering temperatures. We first match the shrinkage profile of the two bulk materials using a Fe_2O_3 sintering additive. Additions of 5 mol% of Fe_2O_3 in the GDC layer and 2 mol% of Fe_2O_3 in the YSZ layer prevents delamination during co-sintering. The addition of Fe_2O_3 promotes densification, enabling achievement of a dense bilayer at a reduced sintering temperature of 1300 °C; ~150 °C below conventional sintering temperatures. Elemental analysis showed the compositional distribution curves across the bilayer interface to be asymmetric when Fe_2O_3 is employed. The Fe_2O_3 increases the total conductivity of the bilayer electrolyte by an order of magnitude; this is explained by the effect of Fe_2O_3 on reducing the resistive solid solution interlayer at YSZ/GDC interface from ~15 to ~5 μm.

1. Introduction

Solid oxide electrolysis cells (SOECs) are important electrochemical devices that can be used for energy storage by converting electrical into chemical energy [1,2]. Research on SOECs has focused largely on water reduction for hydrogen production and significant development has been achieved in recent years [3,4]. In addition to steam electrolysis for hydrogen production, SOECs have also been demonstrated to be feasible for co-electrolysis of CO_2 and H_2O for syngas (H_2 and CO) production [5–7]. In principle, co-electrolysis with a Fischer-Tropsch (F-T) process could convert/store wind or nuclear electrical energy into synthetic fuel by utilising CO_2 as a feedstock.

High performance Solid Oxide Cells (SOC) typically consist of a fuel electrode support with a thin yttria-stabilised zirconia (8YSZ) electrolyte used to minimise the ohmic electrolyte contribution. However, it is argued that electrode supported cells could suffer from an increasing effect of diffusion polarisation due to the larger CO_2 molecules and this may be more vulnerable towards carbon deposition [8,9]. If sufficient ionic conductivity can be achieved, electrolyte supported cells are an interesting configuration to be further investigated due to ease of manufacturing.

Gadolinium-doped ceria (GDC10) is considered to be a promising electrolyte material [10]. Whilst GDC10 has higher oxide ion conductivity than 8YSZ, it suffers from mixed ionic and electronic conduction due to the partial reduction of Ce^{4+} to Ce^{3+} during operation which is detrimental to cell performance [11]. A bi-layer GDC10/8YSZ composite electrolyte could enable high power/current density SOCs [12,13] by utilising the higher ionic conductivity of GDC10 whilst preventing electronic leakage by using an 8YSZ blocking layer. This geometry will prevent partial reduction of GDC and increase the chemical stability of ceria by separating it from the fuel reduction environment [14,15]. The interfacial Po_2 can then be controlled by the thickness ratio of the component layers as illustrated in Fig. 1. This is a requirement for designing a chemically stable bilayer electrolyte with minimum electronic conductivity. In addition, further reduction of the bilayer ASR value could also be achieved by minimising the thickness of the YSZ layer [16]. While the bilayer electrolyte concept is promising, bilayer electrolyte fabrication via cost effective wet ceramic processing has proven to be challenging [17,18]. This is due, in part, to the difficulty in depositing a YSZ layer on GDC due to shrinkage mismatch that occurs during co-sintering of the layers. The shrinkage mismatch introduces mechanical defects such as warpage and delamination at the interface [19,20]. In addition, a difference in thermal expansion coefficient for each layer leads to residual stresses within the bi-layers [21–23]. Furthermore, a resistive solid solution phase can form at the YSZ/GDC interface at

* Corresponding authors.
E-mail addresses: a.mehranjani@gmail.com (A.S. Mehranjani), r.rothman@sheffield.ac.uk (R.H. Rothman).

http://dx.doi.org/10.1016/j.jeurceramsoc.2017.05.018

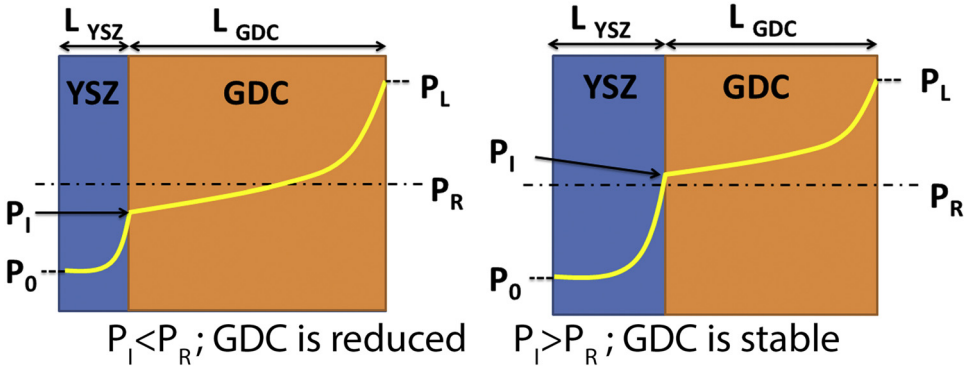

Fig. 1. Schematic of a bilayer electrolyte illustrating the effect of relative thickness on interfacial oxygen partial pressure, P_I, where P_0 is the low pressure p_{o_2} at the fuel/reducing side, P_L is the high pressure p_{o_2} on the air/oxidising side and P_R is the critical p_{o_2} pressure for GDC reduction.

sintering temperatures above 1400 °C [14,24–26]. In general, manufacturing of composite electrolytes by commercial wet ceramic techniques, such as tape casting and screen printing, where materials are subjected to a high co-sintering temperature (≥1400 °C) is limited by deleterious interfacial reactions.

The compositional change at the interface region of GDC/YSZ could dramatically change the electrical performance of the cell. The electrical conductivity of the solid solution phase is reported to be about two orders of magnitude lower than the zirconia electrolyte and one to two orders of magnitude lower than that of Samaria-doped Ceria (SDC) [27]. The thickness of the interdiffusion layer formed at the YSZ/GDC interface plays a key role in the total resistance value. Since interdiffusion is a process which is thermally activated, reduction of sintering temperature and also the sintering time could be an effective approach in limiting the interdiffusion effect.

Tsoga et al. [28] have investigated the elemental diffusion behaviour across the interaction zone using Energy and Wavelength Dispersive X-ray analysis (EDS and WDS, respectively). They prepared samples using screen-printing and sintering at 1400 °C in air for 4 h. Their results indicated a higher diffusion rate of Ce and Gd cations inside the YSZ lattice compared with that of the counter-diffusing Zr and Y cations. Most recently Liang et al. [25] investigated the use of GDC as a diffusion barrier on a Sc-stabilised zirconia (SSZ) electrolyte to mitigate the formation of zirconate from zirconia reacting with cobalt-containing perovskite air electrodes. The authors developed a multi-step sintering process where one layer is first sintered before the next layer is applied, and claimed this approach would reduce the effect of interdiffusion due to the asymmetric diffusion phenomenon at the interface. Liang et al. [25] further suggested that Ce or Gd diffusion towards the SSZ electrolyte would be more difficult due to the already dense microstructure of SSZ and the short dwelling time used.

Zhang et al. [14] fabricated an SSZ/GDC bilayer electrolyte using screen printing and tape casting and fired at 1400 °C for 2 h. Using impedance spectroscopy, they reported an interdiffusion length of ~1 μm and a reduction in total resistance R_{el} by a factor of ~3 in comparison to the reported value of 0.283 Ω cm^2 for a SSZ/GDC bilayer sintered at the same sintering temperature but for 4 h [29]. Wang et al. [29] showed an interdiffusion zone of about 3 μm using EDS analysis. Alternative processing techniques such as pulsed laser deposition (PLD) where high sintering temperatures are not required have also been investigated [30,31] for bilayer electrolyte fabrication; however, these techniques are not cost effective and are difficult to implement for large-scale production. Using transition metal oxides (TMO) as sintering aids is another option to promote densification at lower sintering temperatures [32–36]. Among the various TMO's tested, Fe_2O_3 is reported as a good sintering aid which could improve the conductivity of GDC10 and 8YSZ [32,37].

Here we present the use of Fe_2O_3 as a sintering aid for matching the shrinkage profile of the two bulk materials in a bilayer 8YSZ/GDC electrolyte. Tape casting and one-step, reduced temperature co-sintering are used to fabricate the electrolyte support. We also investigate whether Fe_2O_3 could sufficiently reduce the co-sintering temperature to avoid the formation of a resistive solid solution interlayer. Achieving this objective provides a more cost effective approach for efficient electrolysis of steam and carbon dioxide to produce syngas, where CO_2 could be directly recycled to hydrocarbon fuels for future transportation applications.

2. Experimental procedure

In this study both pellet and tape cast samples were prepared and characterised. Pellet samples were used to study the shrinkage behaviour of the two bulk materials (8YSZ and GDC10) used in the bilayer electrolyte. Tape cast samples were used to fabricate the bilayer support and to study the effects of Fe-dopant and the sintering temperature on the densification behaviour. Electrical measurements were performed on tape cast samples.

GDC10 ($Gd_{0.1}Ce_{0.9}O_{1.95}$) powder (Fuel Cell Materials, US) and 8YSZ ($(Y_2O_3)_{0.08}(ZrO_2)_{0.92}$) powder (TC grade, Tosoh, Japan), were used as starting materials. 2 and 5 mol% of α-Fe_2O_3 (>99%, Sigma-Aldrich) was weighed and added to dry powders before mixing in Isopropanol (>99%, Sigma-Aldrich) for 2 h, using zirconia (ZrO_2) milling media in an attrition mill (model: Szegvari 01HD, Union Process). After milling, the milling media was removed and the suspension dried in a polypropylene jar at 80 °C in a drying oven. After drying, the 5 mol% Fe-GDC10 was ground and calcined in air at 1000 °C for 2 h. The resulting powders were ground and sieved before being pressed into pellets (8 mm diameter, 10 mm thickness), followed by cold iso-pressing (model: CIP-BS EN-286, Vessel Technology) at 150 MPa for 2 min. The shrinkage behaviour for each powder was studied using push rod dilatometry (Netzsch 402C, Germany). All measurements were carried out under air with a flow rate of 30 ml/min between 25 and 1400 °C at a constant heat rate (CHR) of 5 °C min^{-1} and a push rod force of 30 cN. The density of sintered samples was determined using the Archimedes principle and the dimension measurements of the samples. Phase purity of the samples at room temperature were determined using an X-ray diffractometer (model: Bruker D5000, Siemens) over the angular range of 10–80° using a step size of 0.04° and an integration time of 60 s per step. Lattice parameter values and unit-cell volumes were calculated from the most intense (111) reflection using $WinX^{POW}$ software.

Please cite this article in press as: A.S. Mehranjani, et al., Low-temperature co-sintering for fabrication of zirconia/ceria bi-layer electrolyte via tape casting using a Fe_2O_3 sintering aid, *J Eur Ceram Soc* (2017), http://dx.doi.org/10.1016/j.jeurceramsoc.2017.05.018

A tape casting slurry was prepared by mixing the Fe_2O_3 doped powders with polymeric surfactant (Hypermer KD-1) using zirconia balls in an azeotropic mixture (50:50 wt%) of Methyl-ethyl ketone (MEK) and ethanol (EtOH) for 12 h on a ball mill. After milling the suspension was transferred to a polypropylene jar and the milling media removed. Polyvinyl butyral (Butvar B94, Sigma Aldrich) was added as a binder. Butylbenzyl phthalate (Sigma Aldrich) and Polyethylene glycol (Grade 400, Sigma Aldrich) were added as plasticizers. Final mixing was performed using a high shear mixer (DAC 400 FVZ, Speedmixer) with a rotation speed of 2000 rpm and a mixing time of 10 min. This step also de-airs the slip before casting. The tape casting process was performed using a table-top tape caster (Mistler TTC-1200). The slips were cast on a Mylar carrier substrate through a doctor blade gap set at 200 μm at a casting speed of 30 cm/min. The cast slips were left to dry overnight in a drying chamber. Tapes were then laminated using a manual hydraulic press with heated plates (Atlas Manual 15T, Specac) at 85 °C. A pressure of 4 MPa was applied for 15 min while the temperature was kept constant. Tape cast samples with approximately 12 mm diameter and thickness of 100–300 μm, were polished manually using 1200 grit sand paper before applying electrodes. Organo-gold (Au) electrodes were painted and sintered at 800 °C for 1 h.

Impedance measurements were recorded using a Solartron ModuLab Frequency Response Analyser over the range of 0.1 Hz–1 MHz with an applied voltage of 100 mV. Measurements were recorded as a function of temperature between 100 and 500 °C in air. Impedance measurements are presented as impedance complex plane, Z* plots and/or as M" or combined Z", M" spectroscopic plots. The analysis was based on a methodology proposed for analysing impedance data on heterogeneous ceramics by Irvine et al. [38] where each electrically distinct component is represented by a parallel Resistor-Capacitor (RC) element and these are connected in series to create an equivalent circuit to extract R and C values for each component. Different impedance formalisms highlight different aspects of the data, with Z" spectroscopic plots highlighting elements with large R and M" spectroscopic plots identifying elements with small capacitance (normally the bulk (or grain) component), see ref [38] for more details. In principle, each element should give rise to a Debye peak in both Z" and M" spectroscopic plots at the same frequency, f_{max}, and the Debye peaks for the various elements are separated in frequency dependent on their time constant, $\tau = RC$. For each Debye peak, the relationships at the peak maxima are $M''_{max} = \varepsilon_0/2C$ where ε_0 is the permittivity of free space and $Z''_{max} = R/2$ and these allow direct evaluation of C and R, respectively. Using the relationship $\omega RC = 1$ at the Debye peak maximum (where $\omega = 2\pi f_{max}$ and f is the applied frequency in Hz) allows R and C to be estimated from M" and Z" spectra, respectively. Combining M" spectra with Z" spectra or Z* plots that are dominated by RC elements with the largest resistance allows valuable information to be determined regarding conductive/resistive and thick/thin layer elements in multicomponent systems such as bilayered electrolytes. Furthermore, τ (and therefore f_{max}) is a geometry independent parameter ($= \varepsilon_{o\varepsilon}'/\sigma$, where ε' and σ are the permittivity and conductivity of the material, respectively) and is characteristic for a material with given electrical properties.

An Inspect F with a Field Emission Gun, FEI scanning electron microscope (SEM) equipped with an Oxford link pentafet energy dispersive X-ray analyser (EDS) was used for microstructural and compositional analysis. All SEM samples were cold mounted in epoxy resin in cross-sectional orientation before being ground and polished using an Automet 250 Buehler grinding machine, with standard metallographic techniques, and coated with a thin film of carbon to provide electrical conductivity.

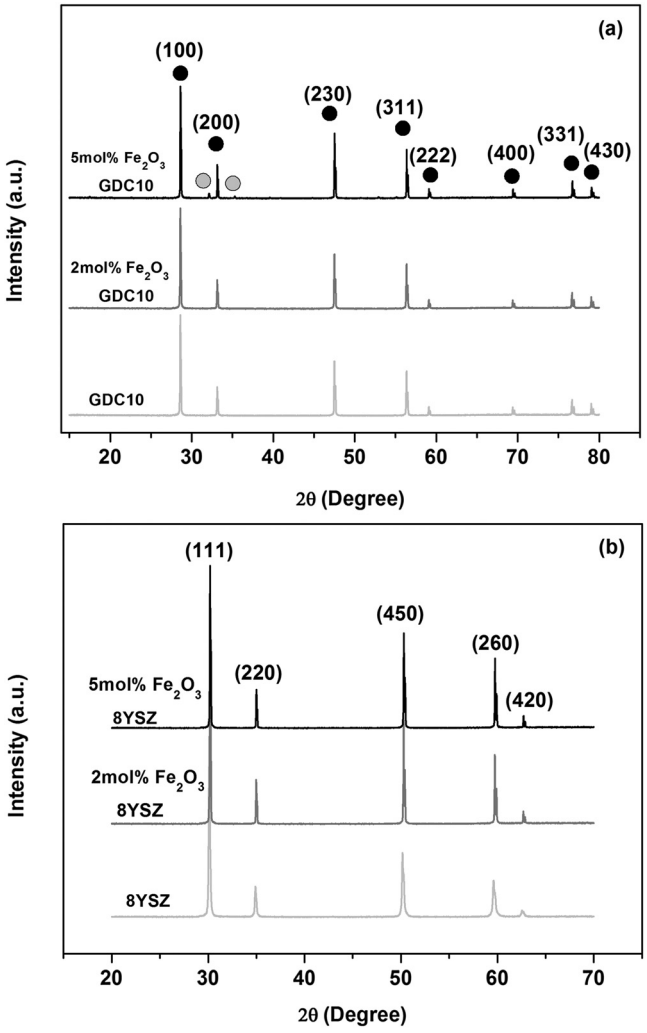

Fig. 2. XRD diffractograms for samples with and without Fe_2O_3 additions sintered at 1250 °C for 4 h (a). GDC10 and (b) 8YSZ. Filled grey circles represent peaks associated with Fe_2O_3.

3. Results and discussion

The effect of Fe_2O_3 on the crystal structure for both materials used in the bilayer electrolyte in the case of sintering at 1250 °C is described in Section 3.1. Section 3.2 describes the effects of Fe_2O_3 as a sintering aid on the densification and shrinkage profile for the case where 2 mol% Fe_2O_3 was added to the 8YSZ layer and 5 mol% Fe_2O_3 was added to the GDC10 layer. Section 3.3 investigates the effect of Fe_2O_3 on the elemental diffusion length at the YSZ/GDC interface. The final section presents the electrical properties of the bilayer electrolytes prepared by tape casting and co-fired at 1300 °C.

3.1. Phase composition and crystal structure

XRD patterns of the sintered samples retained the cubic fluorite structure after Fe-doping, Fig. 2. For GDC samples, however, small additional peaks for Fe_2O_3 appear when the addition level reaches 5 mol%, indicating that Fe_2O_3 has limited solubility in GDC. No additional peaks are observed in samples with 2 mol% Fe_2O_3 additive. This may be due to the small amount of additive which cannot be detected by XRD. Moreover, no secondary phase α-Fe_2O_3 peaks were observed for 5 mol% Fe_2O_3-8YSZ.

Lattice parameter values are summarised in Table 1. The lattice parameter of GDC samples decreases with increasing Fe_2O_3 addi-

Please cite this article in press as: A.S. Mehranjani, et al., Low-temperature co-sintering for fabrication of zirconia/ceria bi-layer electrolyte via tape casting using a Fe_2O_3 sintering aid, *J Eur Ceram Soc* (2017), http://dx.doi.org/10.1016/j.jeurceramsoc.2017.05.018

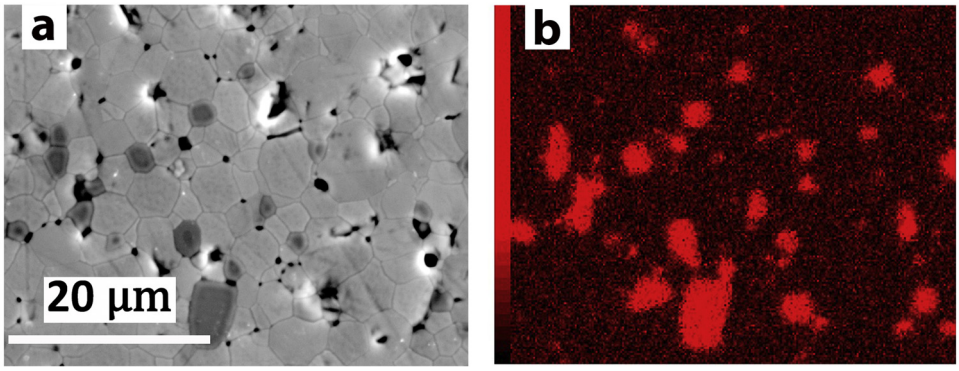

Fig. 3. (a) Back-scattered electron (BSE) image (where dark regions represent iron-rich phase) and (b) the corresponding EDX elemental map (where light regions represent iron-rich phase) for a 5 mol% Fe_2O_3-GDC10 sample sintered at 1200 °C for 4 h.

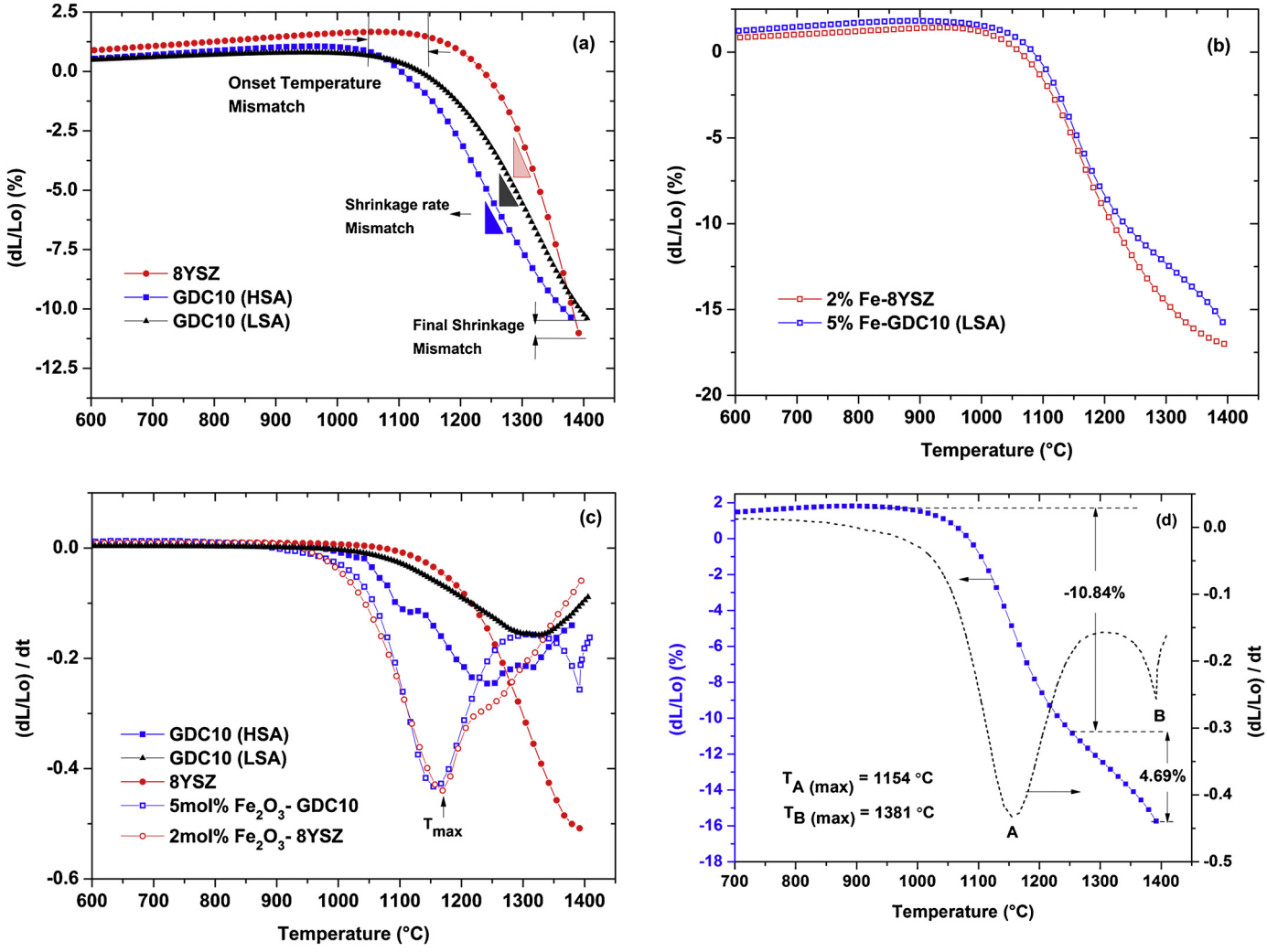

Fig. 4. Constant heat rate dilatometry (CHR) of different powders conducted at 5 °C/min in air. (a) Linear shrinkage as a function of temperature for as-received powders; (b) linear shrinkage as a function of temperature illustrates shrinkage matching; (c) shrinkage rate as a function of temperature for different powders; (d) depicts dual maxima points A and B for 5 mol% Fe_2O_3-GDC10. HSA and LSA refer to high and low surface area powder, respectively.

tions, from 0.5432 to 0.5409 nm; the same trend is observed for 8YSZ. Guo and Xiao [39] also reported a gradual decrease in lattice parameter and unit-cell volume with increasing Fe_2O_3 content. Values reported here confirm those results. The low solubility limit in the case of GDC is rationalized in terms of the severely undersized ionic radius of Fe^{3+} (0.67 Å) versus Ce^{4+} (0.97 Å). The solubility of Fe_2O_3 in Ce_2O_3 is small and reported to be below 1 mol% even at 1500 °C [40,41]. The solubility content of Fe^{3+} in 8YSZ is reported to be 1.5 mol% at 1200 °C [42]. Back-Scattered Electron (BSE) imaging for the 5 mol% Fe_2O_3-GDC10 sample sintered at 1200 °C for 4 h is shown in Fig. 3. The darker grey regions shown in Fig. 3a. represent iron-rich phases. EDX elemental mapping confirmed the Fe-rich phase in the sample, as shown by the red regions in Fig. 3b.

Please cite this article in press as: A.S. Mehranjani, et al., Low-temperature co-sintering for fabrication of zirconia/ceria bi-layer electrolyte via tape casting using a Fe_2O_3 sintering aid, J Eur Ceram Soc (2017), http://dx.doi.org/10.1016/j.jeurceramsoc.2017.05.018

Table 1
Lattice parameter and unit cell volume fraction (ΔV/V%) for samples with different Fe_2O_3 amounts.

Material	Lattice parameter (nm)	ΔV/V (%)
8YSZ	0.5135 ± 0.0011	–
2 mol% Fe_2O_3-8YSZ	0.5076 ± 0.0015	−0.0342
5 mol% Fe_2O_3-8YSZ	0.5069 ± 0.0026	−0.0384
GDC10	0.5423 ± 0.0005	–
2 mol%Fe_2O_3-GDC10	0.5410 ± 0.0011	−0.7174
5 mol% Fe_2O_3-GDC10	0.5409 ± 0.0036	−0.7724

3.2. Shrinkage and densification

The linear shrinkage as a function of temperature for the as-received GDC10 and 8YSZ powders are shown in Fig. 4a. They exhibit different shrinkage behaviour and this is attributed to their different particle morphology and size. The addition of 2 mol% Fe_2O_3 in 8YSZ and 5 mol% Fe_2O_3 in GDC10 reduces the shrinkage mismatch between the two ceramics. However, a further match for the T_{onset} of sintering is achieved by reducing the GDC10 surface area from 8.5 m^2/g (HSA – high surface area) to 1.5 m^2/g (LSA –low surface area) by calcination to coarsen the powder. T_{onset} for both ceramics is well matched at a temperature of ~980 °C after decreasing the GDC10 powder surface area, Fig. 4b. The addition of Fe_2O_3 reduces the temperature of maximum shrinkage (T_{max}) to ~1150 °C as illustrated in Fig. 4c. These results indicate the positive effect of Fe_2O_3 additions in promoting sintering for both 8YSZ and GDC10 ceramics. Furthermore, Fe_2O_3 additions increased the densification rate and led to a narrower temperature range in which most of the sintering is completed.

The formation of an Fe-rich phase due to low Fe-solubility in GDC10 is also apparent from the dilatometry data. The shrinkage rate for 5 mol% Fe_2O_3-GDC10 displays dual maxima points as shown by points A and B in Fig. 4d. The first maximum corresponds to the shrinkage step of ~10 $\frac{dl}{l_0}$ (%) with a T_{max} of 1154 °C and the second maximum corresponds to ~5 $\frac{dl}{l_0}$ (%) shrinkage with a T_{max} of 1381 °C, as illustrated in Fig. 4d.

T_{max} of the second maximum corresponds to the temperature at which there is a reduction in density for the 5 mol% Fe_2O_3 sample when compared to the 2 mol% Fe_2O_3 sample, shown by an arrow in Fig. 5b,c. Since volatilisation of iron at this temperature is not likely, the reduction in density could not be related to iron additive volatilisation at ~1250 °C. The reduction in apparent density at ~1250 °C is not an actual drop in density but is a consequence of the formation of a lower density iron oxide-rich secondary phase.

Selected micrographs of different samples with and without Fe_2O_3 sintered at 1200 °C for 4 h are shown in 6. The Fe_2O_3 free GDC10 (Fig. 6a) is porous with only 69% relative density. Pores are open and continuous with no obvious sign of grain growth. In contrast, 5 mol% Fe_2O_3–GDC10 (Fig. 6b) has a relative density of ~93% with isolated pores and a larger average grain size. Fe_2O_3-free 8YSZ ceramic is also porous (Fig. 6c) with a relative density of ~78% when 8YSZ with 2 mol% Fe_2O_3 (6.d) displays grain growth and a higher relative density of ~95%. The relative density of various green ceramics as a function of temperature is shown in Fig. 5. The relative density (R.D) was extracted from the dilatometry data at 1400 °C; however, a peak value of ~91 R.D% for ceramics from both powders with Fe_2O_3 additives is achieved after a cooling down step in constant heat rate (CHR) experiments.

These results indicate Fe_2O_3 reduces the sintering temperature and promotes densification of both powders. There are numerous reports in the literature concerning the sintering mechanisms for transition metal oxides (TMO's). Kleinlogel and Gauckler [43], proposed that TMO's could form a liquid film at the grain boundary which can enhance the densification mechanism of GDC by liquid phase sintering. However, the temperature range for the sintering process reported by Kleinlogel et al. is within ~50 °C whereas in Fig. 4d it is apparent that the temperature range where sintering occurs is too broad (~200 °C) to be considered as liquid phase sintering. The enhanced sintering behaviour in GDC10 is attributed to an increase in grain boundary Ce^{4+} cation diffusion, whether via liquid or in the solid state.

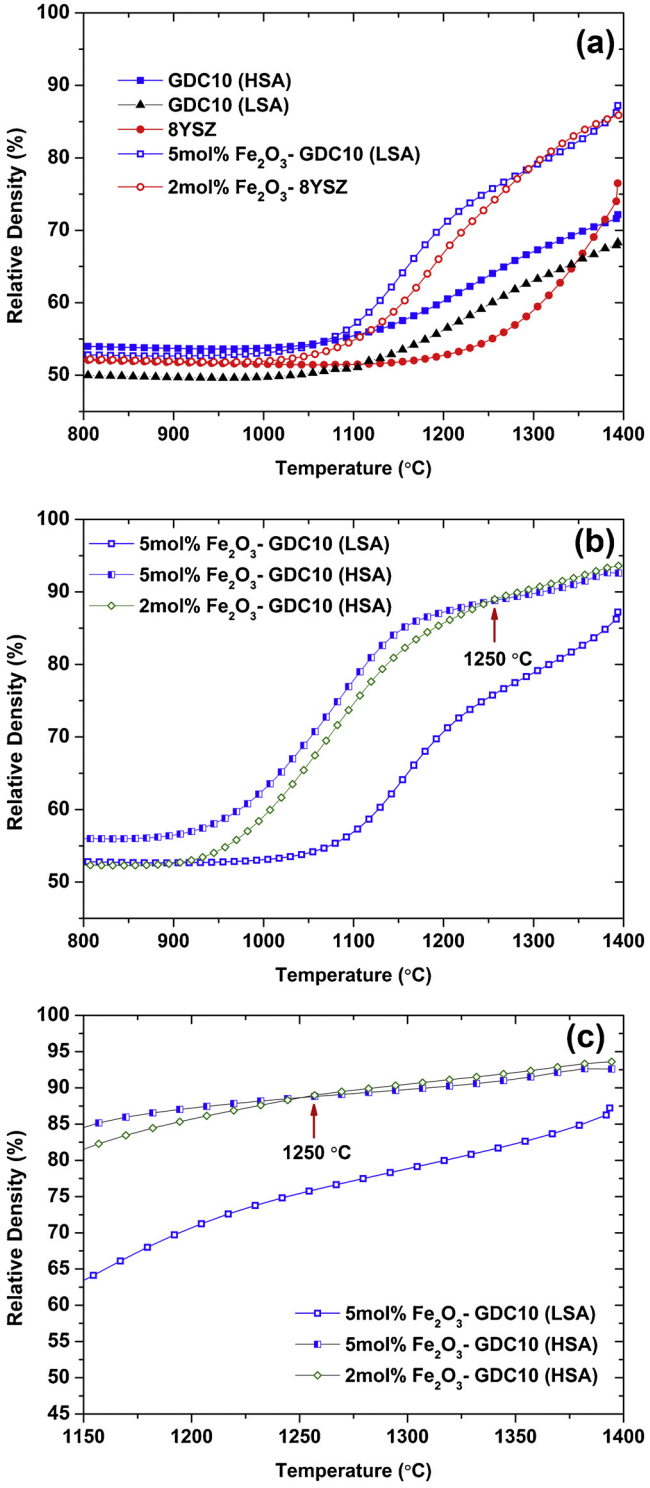

Fig. 5. Relative density versus temperature for various powders, see legend for details. Data from CHR dilatometry conducted at 5 °C/min in air. Arrow shows the reduction in density for a 5 mol% Fe_2O_3-GDC10 sample at 1270 °C.

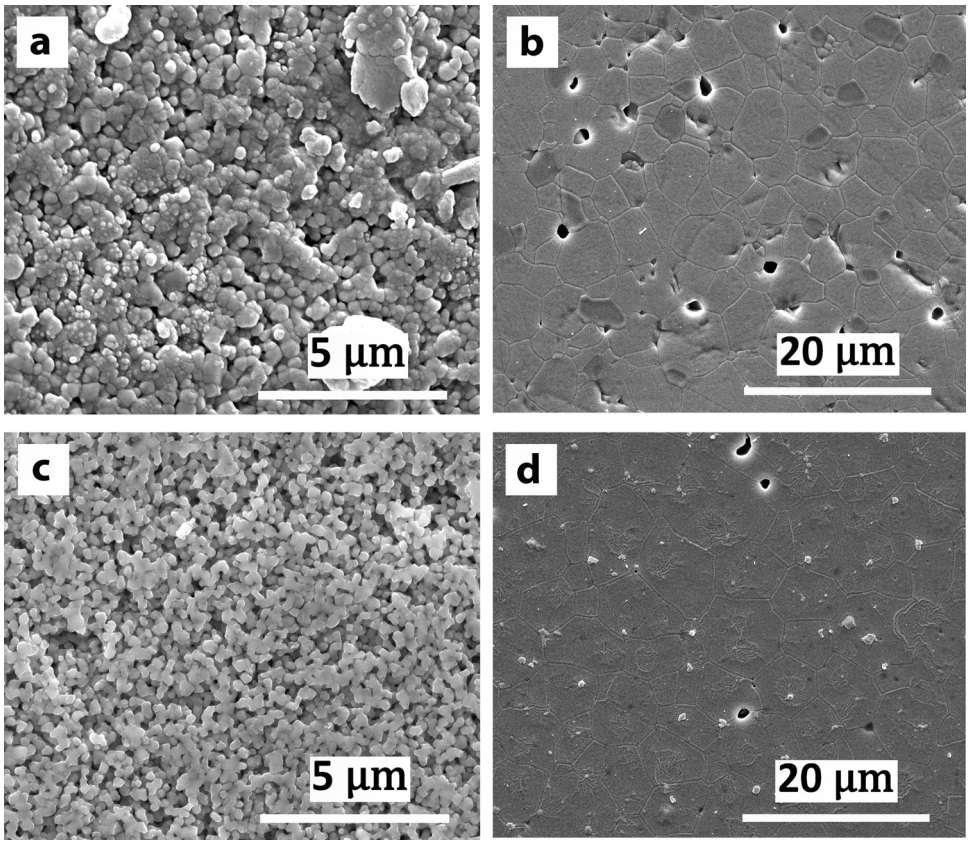

Fig. 6. SEM micrographs of a (a) GDC10 sample without Fe_2O_3; (b) GDC10 with 5 mol% Fe_2O_3; (c) 8YSZ without Fe_2O_3; and (d) 8YSZ with 2 mol% Fe_2O_3. All samples were sintered at 1200 °C for 4 h.

3.3. GDC10/8YSZ microstructure and reactivity

SEM micrographs of the cross sections and relative thickness of two bilayer samples studied are shown in Fig. 7. Samples containing Fe_2O_3 additive are shown in Fig. 7a,b. These micrographs show dense and crack-free bilayers fabricated using tape casting and one step co-sintering and are also characterised by good adhesion at the 8YSZ/GDC10 interface. The digital photograph for the Fe_2O_3 containing bilayer is shown at room temperature in Fig. 8, showing no curviture development after sintering at 1300 °C for 4 h. Fe_2O_3-free samples showed significant delamination between the layers, curvature development and also poor sinterability. To prepare Fe_2O_3-free bilayer samples suitable for EDX measurement an adhesive GDC10 layer with a higher amount of binder content was introduced between the GDC10 and 8YSZ layers when co-sintered as this significantly reduced delamination at the interface as shown in Fig. 7c,d. A back-scattered electron (BSE) image Fig. 7a shows the interdiffusion layer at the 8YSZ/GDC10 interface. The grey regions represent an iron-rich phase and black regions are pores. The GDC10 is identified as the more porous side of the interface. Between the 8YSZ and GDC10 a well densified zone is observed, as presented as a slightly lighter region, and is indicated by the double headed arrow in Fig. 7a. Measurements of the EDS elemental mapping across the interface suggest this zone to be a solid solution between 8YSZ and GDC10, formed during sintering. The EDS elemental mapping in Fig. 9 shows Ce (blue) mainly in the GDC layer, Zr (red) mainly in the YSZ layer. Fig. 9b also suggests more interdiffusion of Zr and Ce at the interface in comparison with Y and Gd. This was also confirmed with EDS line scans taken at 10 different regions near the YSZ/GDC interface for both bilayer samples.

The atomic distributions of Zr, Y, Ce and Gd ions across the interface as a function of distance are shown in Fig. 10. The overall interdiffusion length is estimated as the distance where the atomic% of each element reached between 5 and 90% of their maximum values. This length decreased from ~15 μm in Fe_2O_3-free samples to ~5 μm in samples with Fe_2O_3 additive. The reduced interdiffusion in the Fe_2O_3-containing samples is shown by EDS analysis (Fig. 10). The diffusion behaviour for both Zr and Ce ions in the Fe_2O_3-free bilayer seems to be symmetrical; Bano et al. [26] have also reported an equal interdiffusion length for both Zr and Ce ions in YSZ/GDC bilayer samples co-sintered at 1400 °C for 3 h. However, asymmetric diffusion behaviour is observed for Zr and Ce ions in bilayer samples with Fe_2O_3 additives as shown in Fig. 10a. The interdiffusion length of Zr ions in the GDC layer is ~4 μm and is somewhat larger than that of the diffusion of Ce ions in the YSZ layer, which is ~2 μm.

The results presented for the Fe_2O_3 containing bilayers demonstrate that Fe_2O_3 affects not only the interdiffusion length via reducing the sintering temperature but also that the elemental distribution behaviour for Zr and Ce ions becomes asymmetric. Similar asymmetric diffusion behaviour was reported recently by Tao et al. [25] where multi step sintering was adopted to fabricate SSZ/GDC bilayer electrolytes. Tao et al. [25] suggested the diffusion of Ce or Gd ions (surface diffusion along pores or inter diffusion along grain boundaries) towards the YSZ electrolyte is more difficult due to the already dense micro-structure of YSZ. The diffusion coefficients of Zr ions at ~1400 °C in grains and along the grain boundaries of SSZ are reported to be ~2.8×10^{-15} and 4.8×10^{-8} $cm^2\ s^{-1}$, respectively [44]. Thus Zr diffusion towards the GDC side would be preferential at the grain boundaries. The asymmetric diffusion behaviour in the Fe_2O_3-bilayer could be due to the effect of the Fe_2O_3 concentration on the grain boundary chemistry. It was shown that

Please cite this article in press as: A.S. Mehranjani, et al., Low-temperature co-sintering for fabrication of zirconia/ceria bi-layer electrolyte via tape casting using a Fe_2O_3 sintering aid, *J Eur Ceram Soc* (2017), http://dx.doi.org/10.1016/j.jeurceramsoc.2017.05.018

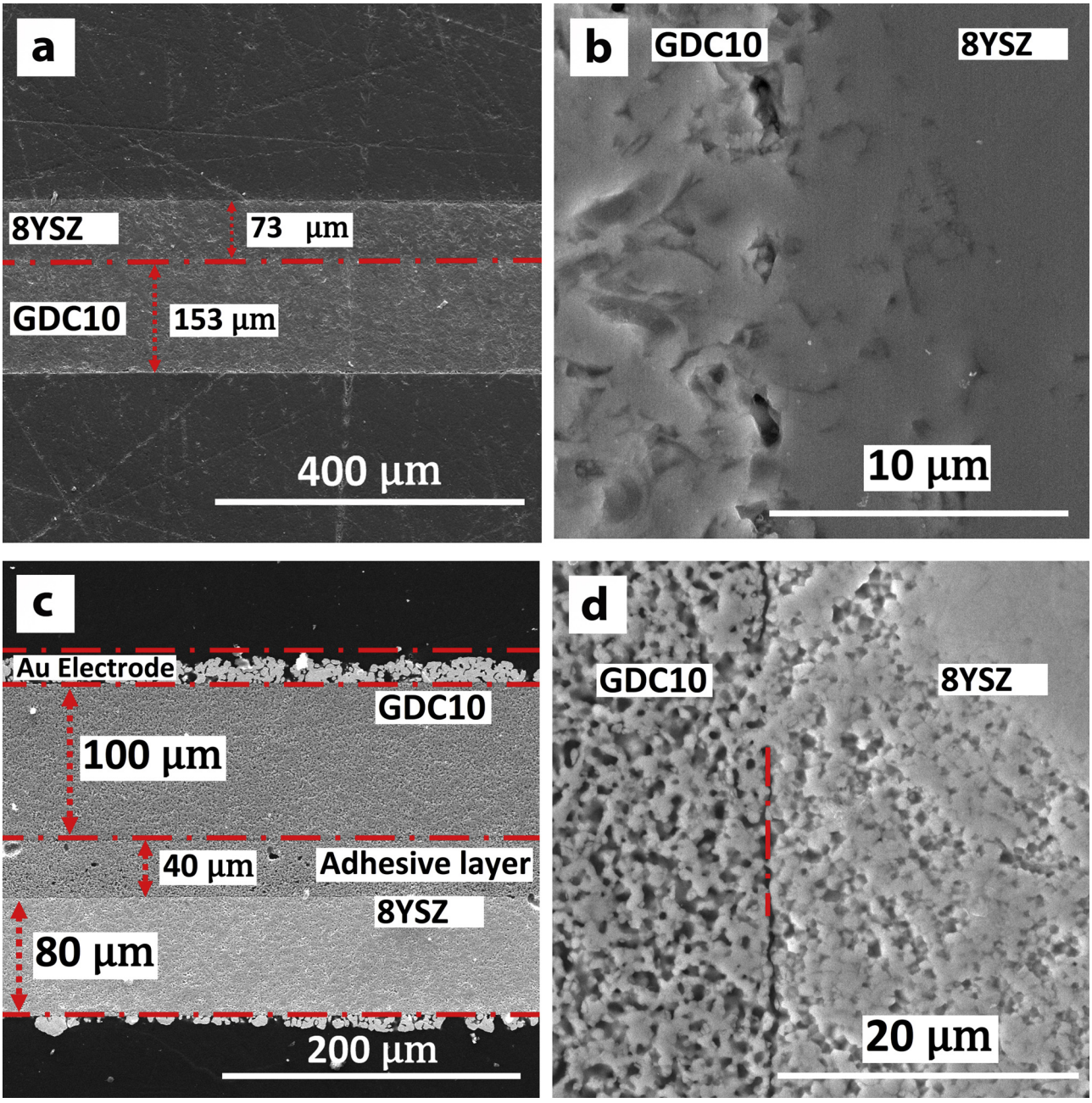

Fig. 7. (a, b) SEM cross section micrograph of Fe_2O_3- YSZ/GDC bilayer sintered at 1300 °C for 4 h and (c,d) Fe_2O_3-free YSZ/GDC bilayer sintered at 1400 °C for 4 h and used for EDX analysis.

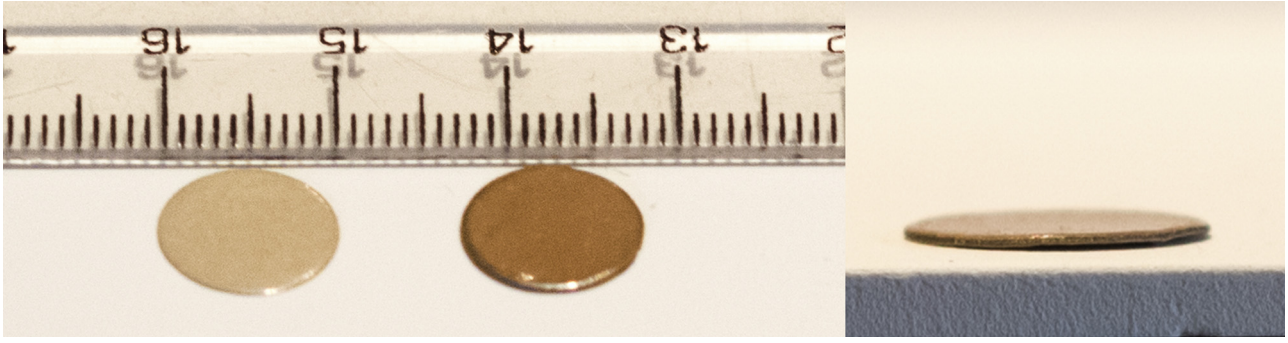

Fig. 8. The digital photograph of Fe_2O_3- YSZ/GDC bilayer sintered at 1300 °C for 4 h at room temperature.

Please cite this article in press as: A.S. Mehranjani, et al., Low-temperature co-sintering for fabrication of zirconia/ceria bi-layer electrolyte via tape casting using a Fe_2O_3 sintering aid, *J Eur Ceram Soc* (2017), http://dx.doi.org/10.1016/j.jeurceramsoc.2017.05.018

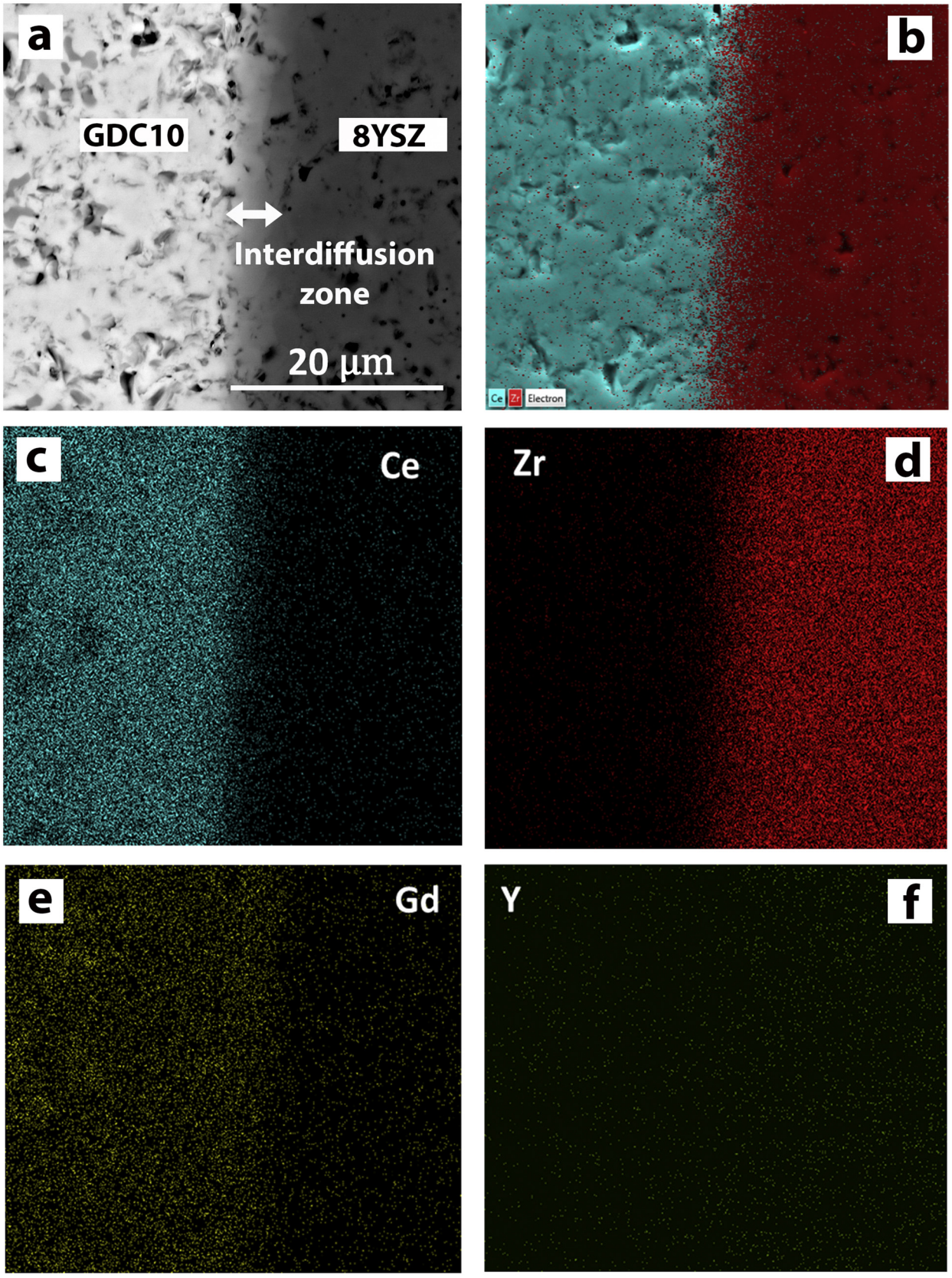

Fig. 9. (a) Back-Scattered Electron (BSE) image of a 5 mol% Fe_2O_3-8YSZ/GDC10 sample sintered at 1300 °C for 4 h; (b) EDS element mapping for the Fe_2O_3- bilayer sintered at 1300 °C for 4 h; (c) elemental mapping for Ce in blue; (d) elemental mapping for Zr in red; (e) elemental mapping for Gd in yellow; and (f) elemental mapping for Y in green.

Please cite this article in press as: A.S. Mehranjani, et al., Low-temperature co-sintering for fabrication of zirconia/ceria bi-layer electrolyte via tape casting using a Fe_2O_3 sintering aid, *J Eur Ceram Soc* (2017), http://dx.doi.org/10.1016/j.jeurceramsoc.2017.05.018

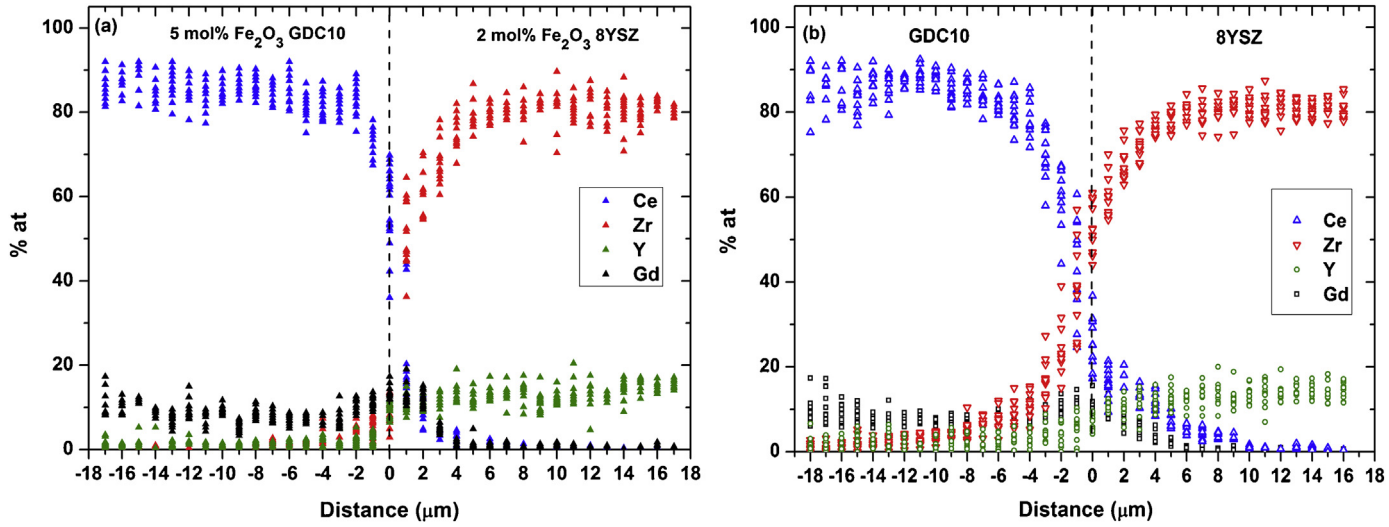

Fig. 10. (a) EDS line scan across a YSZ/GDC interface for a bilayer with Fe_2O_3 additive sintered at 1300 °C for 4 h and (b) an Fe_2O_3-free bilayer sintered at 1400 °C for 4 h.

using 5 mol% Fe_2O_3 additions (above the solubility limit for GDC10) results in segregation of undissolved Fe_2O_3 at the grain boundaries. An increase in the activation energy for grain boundary (GB) conduction in 5 mol% Fe_2O_3-GDC10 from 0.89 ± 0.03 eV to 1.02 ± 0.02 eV from impedance measurements (not shown) also provides evidence that the nature of the GB phase has changed. It is proposed that Fe segregation at the GB core may act as a diffusion barrier for Zr and Y ions. Direct evidence for this suggestion requires analytical Transmission Electron Microscopy to provide information about the location and concentration of iron at the grain boundaries. It is challenging to avoid such ionic diffusion at the atomic level, especially when high sintering temperatures are required for electrolyte fabrication.

3.4. Electrical properties

The electrical properties of bilayer samples were also analysed to investigate the effect of Fe_2O_3 on the performance of the bilayer electrolytes. Prior to this analysis, the impedance response of individual electrolyte ceramics, with and without Fe_2O_3 additions were collected and analysed to assist with the interpretation of the impedance response of the bilayers. The Fe_2O_3-free bilayer electrolyte was sintered at 1400 °C for 4 h whereas the Fe_2O_3-containg bilayer was sintered at 1300 °C for 4 h.

M" spectroscopic plots for all samples between 150 and 300 °C are shown in Fig. 11. In the case of the Fe_2O_3-free bilayer, three M" peaks are visible in the spectrum at 150 °C, labelled A, B and C (with decreasing frequency) in Fig. 11a. Each peak has a time constant (and therefore f_{max}) which relates to a distinct electrical component in the bilayer. Comparison of f_{max} values with the response of the Fe_2O_3-free single layer electrolytes reveals peak A in the bilayers is associated with the M" grain (bulk) response of the GDC10 single layer and peak B is associated with the M" grain (bulk) response of the 8YSZ single layer. With increasing temperature, all peaks move to higher frequency such that f_{max} associated with peak A and the M" GDC10 response exceed the maximum frequency recorded (1 MHz) at >150 °C, peak B and the M" 8YSZ response is visible at 200 and 300 °C, and peak C has $f_{max} \sim 100$ Hz at 300 °C (Fig. 11b and c). A Z* plot of the same data at 300 °C reveals a single large arc with a Z" f_{max} ~100 Hz and resistivity of ~2.75 MΩ cm, Fig. 12a. The Z" f_{max} value coincides with that from peak C in the corresponding M" data and shows this element to dominate the impedance response of the bilayer. Lower frequency Z* data indicate the presence of electrode related phenomena and therefore the total conductivity, σ_T, of the Fe_2O_3-free bilayer electrolyte can be estimated from the diameter of the single, large arc observed in the Z* data (where $\sigma = 1/R$).

An Arrhenius plot of conductivity values extracted from the three peaks in the M" spectra and from the large arc in Z* plots is shown in Fig. 13. This clearly shows GDC10 (peak A) to be the most conductive element, followed by 8YSZ (peak B) and given the similarity of the conductivity data extracted from the Z* arc and peak C in the M" data, this element dominates the resistance of the bilayer electrolyte. It has been reported that a reduction in the bilayer ceramic conductivity could be due to the formation of a high resistance solid solution at the interface between GDC and YSZ layers in bilayer electrolytes [14,25,26]. The equivalent circuit for the Fe_2O_3-free bilayer electrolyte ceramic (neglecting the low frequency electrode response) can therefore be approximated to three, parallel RC elements connected in series; these are GDC10 (peak A), 8YSZ (peak B) and a resistive interdiffusion layer associated with the Ce/Zr solid solution phase (peak C).

In contrast, only two M" peaks are observed in the spectrum of the Fe_2O_3-containing bilayer electrolytes at 150 °C (Fig. 11d). The f_{max} of peak A is coincident with that observed for the 5 mol% Fe-GDC10 single layer ceramic, confirming this to be the same element in both samples; however, although f_{max} for the M" peak B in the bilayer occurs at a similar frequency to that observed for the 2 mol% Fe-8YSZ single layer ceramics, it occurs at a lower frequency, indicating that τ is significantly different for these two components (Fig. 11d). Again, increasing temperature results in f_{max} for the M" peak A exceeding 1 MHz and moving off-scale at higher frequency, whereas f_{max} for the M" peak B remains within the measured frequency range with f_{max} ~70 kHz at 300 °C (Fig. 11e,f). A Z* plot of the same data at 300 °C reveals two overlapping asymmetric arcs with the lower arc dominating the response of the ceramic and this is followed by low frequency electrode phenomena, Fig. 12b.

Based on the Z* data, the total resistivity of the Fe-containing bilayer at 300 °C is ~270 kΩ cm, Fig. 12b. The Z" f_{max} value for the lower frequency arc coincides with that from peak B in the corresponding M" data and confirms this element to dominate the impedance response of the Fe-containing bilayer. The electrical resistivity of the Fe-containing bilayer is an order of magnitude lower than the Fe-free bilayer electrolyte at 300 °C, Fig. 12.

The impedance data and Z* plots provide a simple explanation for the conductivity change which also accompany the EDX results where a reduction in the elemental interdiffusion length was observed in the Fe_2O_3-containing bilayer. On the basis of con-

Please cite this article in press as: A.S. Mehranjani, et al., Low-temperature co-sintering for fabrication of zirconia/ceria bi-layer electrolyte via tape casting using a Fe_2O_3 sintering aid, *J Eur Ceram Soc* (2017), http://dx.doi.org/10.1016/j.jeurceramsoc.2017.05.018

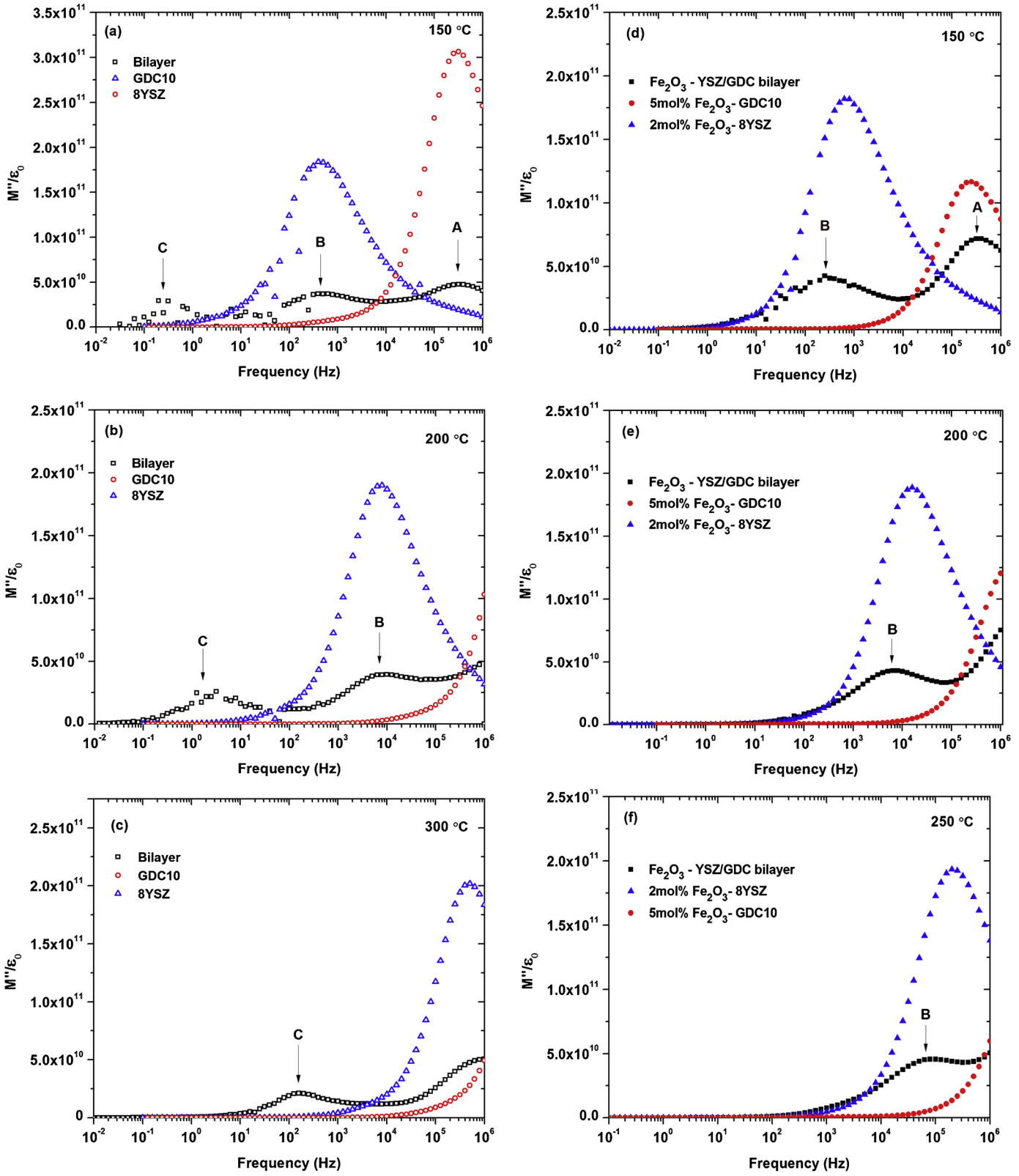

Fig. 11. (a,b,c) M" spectroscopic plots for Fe_2O_3-free bilayer and single layer electrolytes at different temperatures; (d,e,f) M" spectroscopic plots for Fe_2O_3 containing bilayer and single layer electrolytes at different temperatures. Single layer electrolytes are included to identify the bulk (grain) response of the electrolyte layers in the bilayers. M"/ε_o (y-axis) has units of cm/F and Frequency (x-axis) has unit of Hz.

ductivity data alone, it can be inferred that the higher conductivity of the Fe_2O_3-containing bilayer is due to a decrease in the resistive solid solution length. In fact, based on the M" data it is proposed that the increased conductivity can be assigned to the formation of a higher conductive Ce/Zr solid solution composition in the presence of Fe_2O_3. To confirm this hypothesis we compare the f_{max} values

Please cite this article in press as: A.S. Mehranjani, et al., Low-temperature co-sintering for fabrication of zirconia/ceria bi-layer electrolyte via tape casting using a Fe_2O_3 sintering aid, *J Eur Ceram Soc* (2017), http://dx.doi.org/10.1016/j.jeurceramsoc.2017.05.018

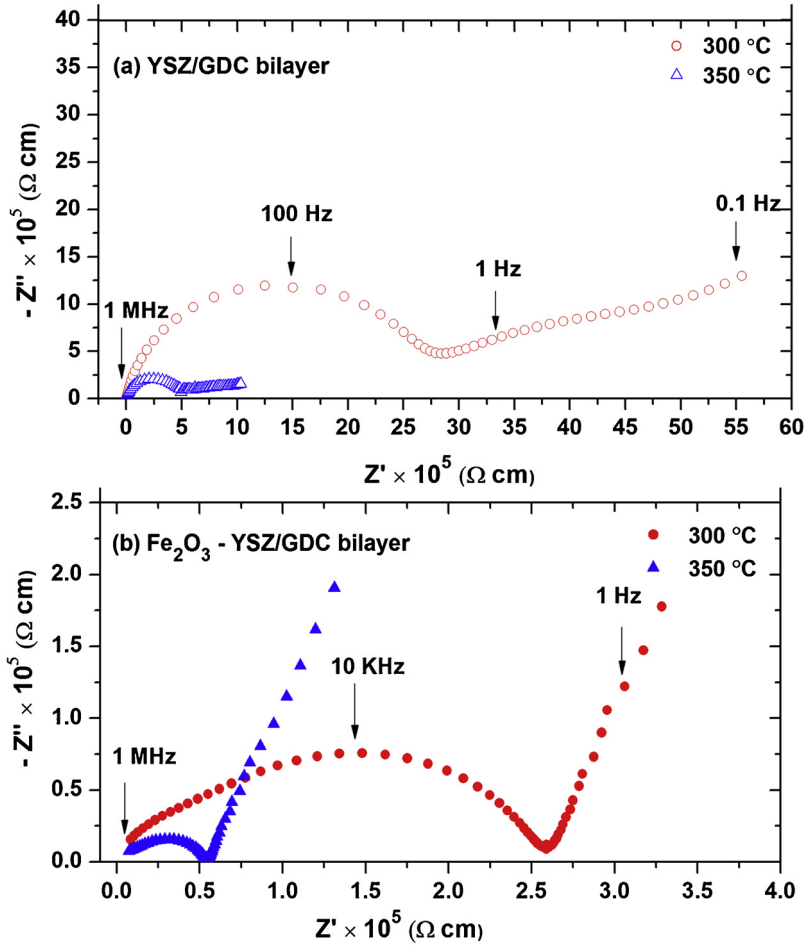

Fig. 12. Z^* plots for bilayers measured in air at different temperatures. (a) Fe_2O_3-free bilayer sample sintered at 1400 °C for 4 h; (b) bilayer with Fe_2O_3 additive sintered at 1300 °C for 4 h. Note the difference in scales for the two graphs.

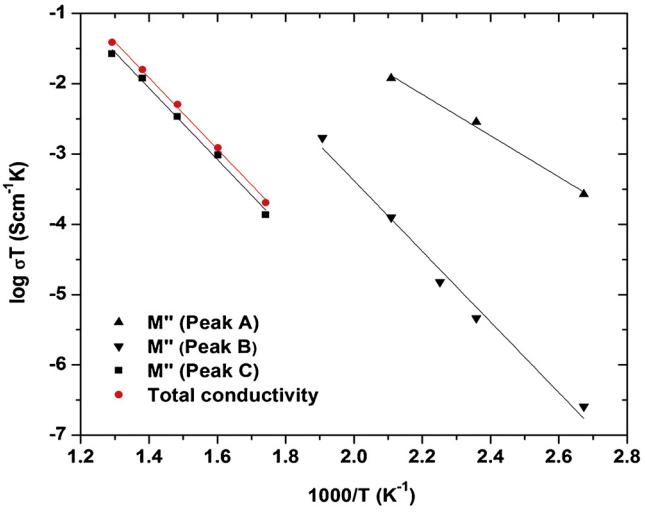

Fig. 13. Arrhenius plot of conductivity for a Fe_2O_3-free bilayer. The total conductivity, σ_T, (filled red circles) has been calculated using Z^* plots and the three components identified by analysing the three peaks in the M'' spectroscopic data. (For interpretation of the references to colour in this figure legend, the reader is referred to the web version of this article.)

obtained from the M" spectra for selected samples across the measured temperature range where impedance data were recorded.

An Arrhenius-type plot of f_{max} values ($\log f_{M''_{max}}$) as a function of reciprocal temperature is shown in Fig. 14 for single layers of 8YSZ and GDC10 with and without Fe-additions and for an Fe-containing bilayer sintered at 1300 °C in air for 4 h. Although only limited data can be collected over the measured frequency and temperature range, f_{max} values for the conductive GDC10 single layer response (with and without Fe-additions) and for peak A in the Fe-containing bilayer are very similar indicating that Fe-additions have very limited influence (if any) on the electrical properties of GDC10. In contrast, there is a significant difference in the f_{max} values for the Fe_2O_3-bilayer (M" peak B) values with the single layer 2 mol% Fe_2O_3-8YSZ ceramic, confirming the electrical response of these materials are similar but distinct, adding evidence for the formation of a resistive solid solution phase with similar composition to 8YSZ.

In an attempt to compare the conductivity values of the two types of Ce/Zr solid solution phases identified in each of the bilayer samples, further analysis of the impedance data was performed. As shown above, the large arc in the Z^* plots and peak C in the M" spectra dominate the sample resistance (and therefore limit the total conductivity, σ_T) for the Fe-free bilayer and can be attributed to the interdiffusion Ce/Zr solid solution phase, Fig. 13. The total bilayer conductivity, σ_T is 0.353 μS cm^{-1} at 300 °C and, by considering the interfacial diffusion length of ~0.0015 cm obtained from the EDX analysis, the sheet resistivity value for the solid solution phase ($R_{interface}$) in the Fe_2O_3-free bilayer is ~4125 Ω cm^2 at 300 °C.

The total resistance of Fe_2O_3- bilayer electrolytes (R_{el}) consists of three parts $R_{el,YSZ}$, $R_{el,GDC}$ and $R_{interface}$. Based on the conductiv-

Please cite this article in press as: A.S. Mehranjani, et al., Low-temperature co-sintering for fabrication of zirconia/ceria bi-layer electrolyte via tape casting using a Fe_2O_3 sintering aid, *J Eur Ceram Soc* (2017), http://dx.doi.org/10.1016/j.jeurceramsoc.2017.05.018

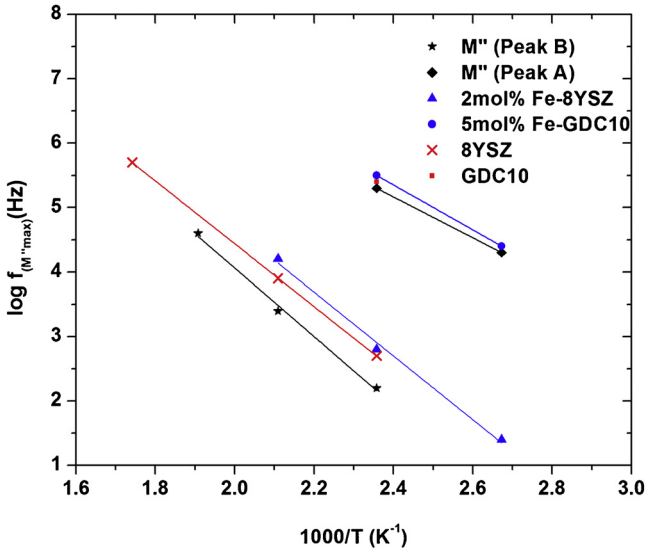

Fig. 14. Arrhenius-type plot of $f_{M"_{max}}$ values as a function of reciprocal temperature for single layer ceramics of 8YSZ (red crosses), GDC10 (filled red circles), 2 mol%Fe-8YZ (filled blue triangles) and 5 mol%Fe-GDC10 (filled blue circles) and for an Fe-containing bilayer sintered at 1300 °C for 4 h with two M" peaks (A (black filled squares) and B (black filled stars). (For interpretation of the references to colour in this figure legend, the reader is referred to the web version of this article.)

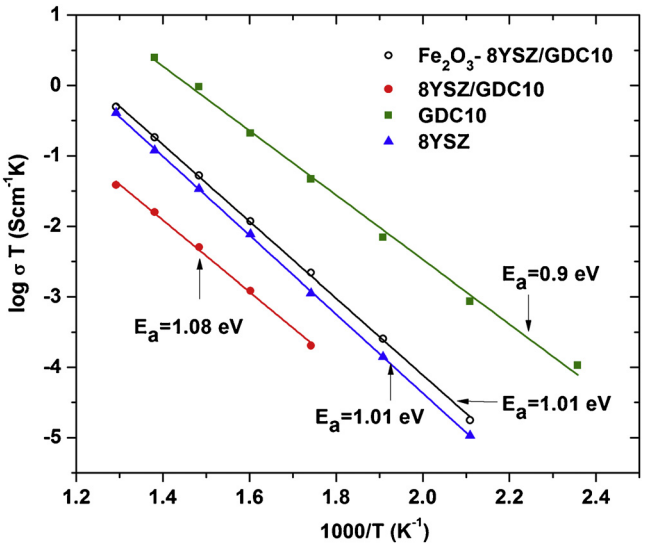

Fig. 15. Arrhenius plot of total conductivity, σ_T, values of the Fe-free bilayer (●) and the Fe_2O_3-bilayer (○) in air. Conductivity values for single layer 8YSZ electrolytes (▲) and GDC10 (■) are included for comparison.

Table 2
Total conductivity (σ_T) and activation energy values measured for different samples, at 500 °C in air. Activation energies for bilayer samples are taken in the temperature range of ~150–500 °C.

Composition	$\sigma_{T(500)}$ S cm^{-1}	$\sigma_{T(300)}$ S cm^{-1}	E_T (eV)
Fe_2O_3-Bilayer	6.44×10^{-4}	3.82×10^{-6}	1.01 ± 0.03
Fe_2O_3-free Bilayer	5.00×10^{-5}	3.53×10^{-7}	1.08 ± 0.02
2 mol% Fe_2O_3-8YSZ	5.23×10^{-4}	2.90×10^{-6}	1.10 ± 0.02
5 mol% Fe_2O_3-GDC10	5.92×10^{-3}	2.10×10^{-5}	0.90 ± 0.01

ity values for 2 mol% Fe_2O_3-8YSZ and 5 mol% Fe_2O_3-GDC10 layers summarised in Table 2, and by considering the thickness ratio of each layer shown in Fig. 7, the contribution of $R_{interface}$ can be estimated (Table 3). $R_{interface}$ for the Fe_2O_3- bilayer is estimated to be ~2670 Ω cm^2 at 300 °C, almost half the value measured for $R_{interface}$ in the Fe_2O_3 –free bilayer sample.

The corresponding Arrhenius plot for conductivity of different samples over the temperature range is given in Fig. 15. These results demonstrate the agreement in conduction behaviour discussed. An increase in σ_T by an order of magnitude is observed for the Fe_2O_3-bilayer in comparison to the Fe_2O_3-free bilayer. The activation energy in the temperature range of ~150–450 °C is also calculated from the slopes and is equal to 1.01 ± 0.02 eV and 1.08 ± 0.03 eV for the Fe_2O_3-bilayer and Fe_2O_3-free bilayer, respectively. The activation energy for the Fe_2O_3-free bilayer electrolyte measured in this work is very similar to the activation energy of 1.1 for the Ce/Zr solid solution reported by Tsoga et al. [28].

The bilayer sintering temperature in this study is 1300 °C which is lower than the temperature of formation of the ceria-zirconia solid solution reported elsewhere in the literature [14,15]; however, it is higher than 1100 °C where a solid solution was reported when using electrostatic spray deposition as the fabrication technique [45]. The results presented here demonstrate that the fabrication of bilayer electrolyte supports for planar SOC's with a YSZ blocking layer is possible by tape casting and co-sintering. The techniques are cost affective and feasible. The interdiffusion at the interface between GDC10 and 8YSZ can be reduced to obtain better electrolyte performance. Future work will focus on cell performance during high temperature electrolysis of CO_2 and steam.

4. Conclusions

Bilayer 8YSZ/GDC10 electrolytes have been successfully fabricated by tape casting and reduced-temperature co-sintering at 1300 °C. No significant microstructural defects or delamination were observed after co-firing. The enhanced densification and shrinkage matching of GDC10 and 8YSZ were achieved by using different amounts of a Fe2O3 sintering aid in the electrolyte layers. Micro-chemical and micro-structural analysis showed that increasing the Fe_2O_3 addition levels above the solubility content leads to formation of an iron-rich phase. EDX analysis revealed asymmetric elemental diffusion behaviour when using Fe_2O_3 to co-sinter YSZ/GDC bilayers, with lower diffusivity of Zr and Y ions in the GDC10 layer compared to that of Ce and Gd ions detected in the 8YSZ layer, showing the positive effect of Fe_2O_3 on limiting the interdiffusion behaviour.

Electrochemical impedance measurements in air revealed the total conductivity of the Fe_2O_3 containing bilayer electrolytes increased by an order of magnitude compared to Fe_2O_3-free bilayers. This was attributed to two factors; first, by limiting the overall elemental interdiffusion length from ~15 to ~5 μm and, second, by achieving better contact between the 8YSZ and GDC10 layers and higher sintered density when using a Fe_2O_3 additive as a sintering aid. Also, the total conductivity of Fe_2O_3 containing bilayer electrolytes is 1.5 times of the single layer 8YSZ electrolyte. This work demonstrates a cost-effective wet ceramic fabrication technique such as tape casting can potentially be used for bilayer electrolyte

Table 3
Estimated sheet resistivity values for a Fe-containing bilayer at 300 °C and 500 °C, calculated from conductivity values in Table 2 and the thickness ratio shown in Fig. 7.

Temperature	R_{el} (Ω cm^2)	R_{GDC} (Ω cm^2)	R_{YSZ} (Ω cm^2)	$R_{interface}$ (Ω cm^2)	$\tau_{interdiffusion}$ (cm)
300 °C	5.92×10^3	7.29×10^2	2.52×10^3	2.67×10^3	0.0005
500 °C	3.51×10^1	2.58	1.40×10^1	1.86×10^1	0.0005

Please cite this article in press as: A.S. Mehranjani, et al., Low-temperature co-sintering for fabrication of zirconia/ceria bi-layer electrolyte via tape casting using a Fe_2O_3 sintering aid, *J Eur Ceram Soc* (2017), http://dx.doi.org/10.1016/j.jeurceramsoc.2017.05.018

cell fabrication; however, additional studies are required to further reduce the effect of interdiffusion between the layers.

Acknowledgements

This work was carried out as part of the 4CU programme grant, aimed at sustainable conversion of carbon dioxide into fuels, led by The University of Sheffield and carried out in collaboration with The University of Manchester, Queens University Belfast and University College London. The authors acknowledge gratefully the Engineering and Physical Sciences Research Council (EPSRC) for supporting this work financially (Grant No EP/K001329/1). The authors also thank Dr Ann Call (University of Sheffield) for technical discussions.

References

[1] T.-R. Lee, H.-N. Im, S.-Y. Jeon, Y.-S. Yoo, A.U. Chavan, S.-J. Song, Dependence of H2O/CO2 Co-electrolysis performance of SOEC on microstructural and thermodynamic parameters, J. Electrochem. Soc. 163 (7) (2016) F728–F736.
[2] H. Xu, B. Chen, M. Ni, Modeling of direct carbon-assisted solid oxide electrolysis cell (SOEC) for syngas production at two different electrodes, J. Electrochem. Soc. 163 (11) (2016) F3029–F3035.
[3] M.A. Laguna-Bercero, R. Campana, A. Larrea, J.A. Kilner, V.M. Orera, Steam electrolysis using a microtubular solid oxide fuel cell, J. Electrochem. Soc. 157 (6) (2010) B852–B855.
[4] J. Koponen, Review of Water Electrolysis Technologies and Design of Renewable Hydrogen Production Systems, LUT School of Energy Systems, Lappeenranta University of Technology, 2015.
[5] C. Graves, S.D. Ebbesen, M. Mogensen, Co-electrolysis of CO2 and H2O in solid oxide cells: performance and durability, Solid State Ionics 192 (1) (2011) 398–403.
[6] M. Ni, An electrochemical model for syngas production by co-electrolysis of H2O and CO2, J. Power Sources 202 (0) (2012) 209–216.
[7] G. Wu, K. Xie, Y. Wu, W. Yao, J. Zhou, Electrochemical conversion of H2O/CO2 to fuel in a proton-conducting solid oxide electrolyser, J. Power Sources 232 (0) (2013) 187–192.
[8] J.-H. Koh, Y.-S. Yoo, J.-W. Park, H.C. Lim, Carbon deposition and cell performance of Ni-YSZ anode support SOFC with methane fuel, Solid State Ionics 149 (3–4) (2002) 157–166.
[9] Y. Tao, S.D. Ebbesen, M.B. Mogensen, Carbon deposition in solid oxide cells during Co-electrolysis of H2O and CO2, J. Electrochem. Soc. 161 (3) (2014) F337–F343.
[10] H. Huang, M. Nakamura, P. Su, R. Fasching, Y. Saito, F.B. Prinz, High-performance ultrathin solid oxide fuel cells for low-temperature operation, J. Electrochem. Soc. 154 (1) (2007) B20–B24.
[11] B.C.H. Steele, Appraisal of Ce 1-yGd yO 2-y/2 electrolytes for IT-SOFC operation at 500 °C, Solid State Ionics 129 (1) (2000) 95–110.
[12] J.S. Ahn, D. Pergolesi, M.A. Camaratta, H. Yoon, B.W. Lee, K.T. Lee, D.W. Jung, E. Traversa, E.D. Wachsman, High-performance bilayered electrolyte intermediate temperature solid oxide fuel cells, Electrochem. Commun. 11 (7) (2009) 1504–1507.
[13] J.S. Ahn, M.A. Camaratta, D. Pergolesi, K.T. Lee, H. Yoon, B.W. Lee, D.W. Jung, E. Traversa, E.D. Wachsman, Development of high performance ceria/bismuth oxide bilayered electrolyte SOFCs for lower temperature operation, J. Electrochem. Soc. 157 (3) (2010) B376–B382.
[14] X. Zhang, M. Robertson, C. Decès-Petit, Y. Xie, R. Hui, W. Qu, O. Kesler, R. Maric, D. Ghosh, Solid oxide fuel cells with bi-layered electrolyte structure, J. Power Sources 175 (2) (2008) 800–805.
[15] P. Kim-Lohsoontorn, N. Laosiripojana, J. Bae, Performance of solid oxide electrolysis cell having bi-layered electrolyte during steam electrolysis and carbon dioxide electrolysis, Curr. Appl. Phys. 11 (Suppl. 1) (2011) S223–S228.
[16] E.D. Wachsman, Functionally gradient bilayer oxide membranes and electrolytes, Solid State Ionics 152–153 (2002) 657–662.
[17] P.Z. Cai, G.L. Messing, D.J. Green, Determination of the mechanical response of sintering compacts by cyclic loading dilatometry, J. Am. Ceram. Soc. 80 (2) (1997) 445–452.
[18] D. Ravi, D.J. Green, Sintering stresses and distortion produced by density differences in bi-layer structures, J. Eur. Ceram. Soc. 26 (1–2) (2006) 17–25.
[19] R.-T. Hsu, J.-H. Jean, Key factors controlling camber behavior during the cofiring of Bi-layer ceramic dielectric laminates, J. Am. Ceram. Soc. 88 (9) (2005) 2429–2434.
[20] P.Z. Cai, D.J. Green, G.L. Messing, Constrained densification of alumina/zirconia hybrid laminates, I: experimental observations of processing defects, J. Am. Ceram. Soc. 80 (8) (1997) 1929–1939.
[21] J. Malzbender, W. Fischer, R.W. Steinbrech, Studies of residual stresses in planar solid oxide fuel cells, J. Power Sources 182 (2) (2008) 594–598.
[22] A. Atkinson, A. Selçuk, Residual stress and fracture of laminated ceramic membranes, Acta Mater. 47 (3) (1999) 867–874.
[23] T.L. Jiang, M.-H. Chen, Thermal-stress analyses of an operating planar solid oxide fuel cell with the bonded compliant seal design, Int. J. Hydrogen Energy 34 (19) (2009) 8223–8234.
[24] T. Kawada, H. Yokokawa, M. Dokiya, N. Sakai, T. Horita, J. Van Herle, K. Sasaki, Ceria-zirconia composite electrolyte for solid oxide fuel cells, J. Electroceram. 1 (2) (1997) 155–164.
[25] B. Liang, T. Tao, S. Zhang, Y. Huang, Z. Cai, S. Lu, Asymmetric diffusion of Zr, Sc and Ce Gd at the interface between zirconia electrolyte and ceria interlayer for solid oxide fuel cells, J. Alloys Compd. 679 (2016) 191–195.
[26] A. Mahmood, S. Bano, J.H. Yu, K.-H. Lee, High-performance solid oxide electrolysis cell based on ScSZ/GDC (scandia-stabilized zirconia/gadolinium-doped ceria) bi-layered electrolyte and LSCF (lanthanum strontium cobalt ferrite) oxygen electrode, Energy 90 (Part 1) (2015) 344–350.
[27] A. Tsoga, A. Gupta, A. Naoumidis, D. Skarmoutsos, P. Nikolopoulos, Performance of a double-layer CGO/YSZ electrolyte for solid oxide fuel cells, Ionics 4 (3) (1998) 234–240.
[28] A. Tsoga, A. Gupta, A. Naoumidis, P. Nikolopoulos, Gadolinia-doped ceria and yttria stabilized zirconia interfaces: regarding their application for SOFC technology, Acta Mater. 48 (18–19) (2000) 4709–4714.
[29] Z. Wang, J. Qian, J. Cao, S. Wang, T. Wen, A study of multilayer tape casting method for anode-supported planar type solid oxide fuel cells (SOFCs), J. Alloys Compd. 437 (1–2) (2007) 264–268.
[30] D. Yang, X. Zhang, S. Nikumb, C. Decès-Petit, R. Hui, R. Maric, D. Ghosh, Low temperature solid oxide fuel cells with pulsed laser deposited bi-layer electrolyte, J. Power Sources 164 (1) (2007) 182–188.
[31] J. Fergus, R. Hui, X. Li, D.P. Wilkinson, J. Zhang, Solid Oxide Fuel Cells: Materials Properties and Performance, CRC Press, 2008.
[32] Q. Dong, Z.H. Du, T.S. Zhang, J. Lu, X.C. Song, J. Ma, Sintering and ionic conductivity of 8YSZ and CGO10 electrolytes with small addition of Fe2O3: A comparative study, Int. J. Hydrogen Energy 34 (19) (2009) 7903–7909.
[33] H. Gao, J. Liu, H. Chen, S. Li, T. He, Y. Ji, J. Zhang, The effect of Fe doping on the properties of SOFC electrolyte YSZ, Solid State Ionics 179 (27–32) (2008) 1620–1624.
[34] R.R. Kondakindi, K. Karan, Characterization of Fe- and Mn-doped GDC for low-temperature processing of solid oxide fuel cells, Mater. Chem. Phys. 115 (2–3) (2009) 728–734.
[35] T. Zhang, P. Hing, H. Huang, J. Kilner, Densification, microstructure and grain growth in the CeO2-Fe2O3 system (0Fe/Ce20%), J. Eur. Ceram. Soc. 21 (12) (2001) 2221–2228.
[36] T.S. Zhang, J. Ma, Y.J. Leng, S.H. Chan, P. Hing, J.A. Kilner, Effect of transition metal oxides on densification and electrical properties of Si-containing Ce0.8Gd0.2O2-δ ceramics, Solid State Ionics 168 (1–2) (2004) 187–195.
[37] O. Bohnke, V. Gunes, K.V. Kravchyk, A.G. Belous, O.Z. Yanchevskii, O.I. V'Yunov, Ionic and electronic conductivity of 3 mol% Fe2O3-substituted cubic yttria-stabilized ZrO2 (YSZ) and scandia-stabilized ZrO2 (ScSZ), Solid State Ionics 262 (0) (2014) 517–521.
[38] J.T.S. Irvine, D.C. Sinclair, A.R. West, Electroceramics characterization by impedance spectroscopy, Adv. Mater. 2 (3) (1990) 132–138.
[39] F. Guo, P. Xiao, Effect of Fe2O3 doping on sintering of yttria-stabilized zirconia, J. Eur. Ceram. Soc. 32 (16) (2012) 4157–4164.
[40] Z. Tianshu, P. Hing, H. Huang, J. Kilner, The effect of Fe doping on the sintering behavior of commercial CeO2 powder, J. Mater. Process. Technol. 113 (1–3) (2001) 463–468.
[41] M. Hrovat, J. Holc, S. Bernik, D. Makovec, Subsolidus phase equilibria in the NiO–CeO2 and La2O3–CeO2–Fe2O3 systems, Mater. Res. Bull. 33 (8) (1998) 1175–1183.
[42] M.J. Verkerk, A.J.A. Winnubst, A.J. Burggraaf, Effect of impurities on sintering and conductivity of yttria-stabilized zirconia, J. Mater. Sci. 17 (11) (1982) 3113–3122.
[43] C.M. Kleinlogel, L.J. Gauckler, Mixed electronic-ionic conductivity of cobalt doped cerium gadolinium oxide, J. Electroceram. 5 (3) (2000) 231–243.
[44] M.A. Taylor, M. Kilo, G. Borchardt, S. Weber, H. Scherrer, 96Zr diffusion in polycrystalline scandia stabilized zirconia, J. Eur. Ceram. Soc. 25 (9) (2005) 1591–1595.
[45] G. Constantin, C. Rossignol, J.P. Barnes, E. Djurado, Interface stability of thin, dense CGO film coating on YSZ for solid oxide fuel cells, Solid State Ionics 235 (2013) 36–41.

Please cite this article in press as: A.S. Mehranjani, et al., Low-temperature co-sintering for fabrication of zirconia/ceria bi-layer electrolyte via tape casting using a Fe_2O_3 sintering aid, *J Eur Ceram Soc* (2017), http://dx.doi.org/10.1016/j.jeurceramsoc.2017.05.018